The geological CO_2 degassing history of a long-lived caldera

Giovanni Chiodini[1], L. Pappalardo[2], A. Aiuppa[3,4], and S. Caliro[2]

[1]*INGV, Sezione di Bologna, via Creti 12, 40128 Bologna, Italy*

[2]*INGV, Sezione di Napoli, via Diocleziano 328, 80124 Napoli, Italy*

[3]*Dipartimento DiSTeM, Università di Palermo, Via Archirafi 36, 90123 Palermo, Italy*

[4]*INGV, Sezione di Palermo, via La Malfa 153, 90146 Palermo, Italy*

ABSTRACT

The majority of the ~100 Holocenic calderas on our planet host vigorously active hydrothermal systems, whose heat and volatile budgets are sustained by degassing of deeply stored magma. Calderas may thus contribute a non-trivial, though poorly quantified fraction of the global budget of magmatic volatiles, such as CO_2. Here, we use original isotopic and petrological results from Campi Flegrei (CF) volcano, in Italy, to propose that hydrothermal calcites are natural mineral archives for the magmatic CO_2 that reacted with reservoir rocks during the geological history of a caldera. We show that CF calcites, identified in core samples extracted from 3km deep geothermal wells, formed at isotopic equilibrium with magmatic fluids having $\delta^{18}O_{H2O}$ of +8.7 to +12.7 ‰, and $\delta^{13}C_{CO2}$ of ~−1.5‰. This inferred "fossil" fluid composition is virtually identical to that of present-day fumaroles, demonstrating stable carbon source during the caldera past (<40 ka) history. We use the mass of calcites stored in the hydrothermal system to estimate that 12 Gt of magmatic CO_2 have reacted with the CF rocks during the caldera history, which corresponds to a time-averaged CO_2 flux of ~800 t d^{-1}. This "long-term" CO_2 flux, the first of its kind in the geological literature, is of the same order of the present-day soil CO_2 degassing flux (1100 ± 200 t d^{-1}). We conclude that the "true" magmatic

23 CO_2 degassing flux from calderas may be severely underestimated if subsurface calcite
24 precipitation is not taken into full account.

25 **INTRODUCTION**

26 Calderas represent the indelible traces of some of the most dramatic volcanic events in
27 the geological record. These depressions, typically kilometers to tens of kilometers wide, are the
28 ultimate consequences of large explosive eruptions that drain tens to thousands of km^3 of
29 magma, in short-lived, occasionally climatic volcanic blasts (Sparks et al., 2005). The majority
30 of these volcanic structures undergo long-lived histories of post-caldera formation activity, with
31 sequences of effusive-explosive eruptions that concentrate inside and fill the depression. Owing
32 to their highly nonlinear and often unpredictable behaviors, calderas represent a major volcanic
33 hazard to populations living in their surroundings.

34 Calderas are often the site of intense hydrothermal circulation (Hurwitz and Lowenstern,
35 2014), so that an escalation of surface degassing activity is usually a primary sign of caldera
36 unrest (Chiodini et al., 2012). Unfortunately however, measuring the rate of gas release from
37 active calderas is complicated by the vigorous interactions between magmatic fluids and
38 hydrothermal aquifers (Symonds and Gerlach, 2001), which typically scrub all sulfur dioxide
39 (that could otherwise be easily detected by UV spectroscopy) from the magmatic gas stream.
40 Magmatic-hydrothermal interactions can also complicate the degassing patterns of even less-
41 reactive magmatic gases such as CO_2, which is commonly dissipated in diffuse, invisible form
42 through degassing structures wide up to some km_2. Even in the most favorable circumstances,
43 the past inventories of caldera-related CO_2 emissions have been based upon observational
44 periods (of days, to exceptionally years) that are disproportionally shorter than timescales
45 (millennia to hundred thousands years) of caldera processes.

One possible way to explore, and possibly reconstruct, the long-term degassing record of calderas is to investigate hydrothermal calcites, that are preserved in active and fossil hydrothermal systems as mineral traces of CO_2 reaction with volcanic rocks. These calcites, formed by conversion of Ca-Al-silicates to calcite in active hydrothermal systems (Giggenbach, 1984), open a window to identifying the isotope composition, and eventually the flux, of the source CO_2 from which they formed.

Here, hydrothermal calcites are used in the attempt to first characterize the long-term CO_2 flux regime of the CF caldera, a large (140 km^2) polygenetic collapse structure located near Naples city (Fig. 1). The CF volcano has been the locus of the most catastrophic eruption in the Mediterranean area, the 40ka old Campanian Ignimbrite super-eruption (Volcanic Explosivity Index 7), and has more recently produced (lately in 1538 AD) tens of explosive eruptions in an area counting today more than 350,000 inhabitants. Geophysical anomalies detected by seismic tomography (Zollo et al., 2008) indicate that a partial melting zone is currently present at 7–8 km depth beneath the CF as well as beneath the neighboring Vesuvius volcano; this evidence, consistent with the similarity in petrological features of magmas, suggests that a wide magma source may be active beneath the whole Neapolitan volcanic district (Pappalardo et al., 2008; Pappalardo and Mastrolorenzo, 2012). The caldera has shown signs of unrest since the 1950s (Del Gaudio et al., 2010), and a visible escalation of surface CO_2 degassing during the last years. Degassing is particularly intense in the hydrothermal sites of Solfatara and Pisciarelli (SP), in the caldera center (Fig. 1), which show intense soil diffuse (~1000–1500 t d^{-1}) and fumarolic (~500 t d^{-1}) CO_2 degassing and heat release (~100 MW, Chiodini et al., 2010).

In the attempt to reconstruct the origin and flux of the fluids that deposited hydrothermal calcite in the past volcanic history of CF, we have conducted a petrological and isotopic ($\delta^{13}C$,

69 $\delta^{18}O$) study on 15 core samples from 3 geothermal wells drilled into the upper 3 km of the
70 caldera (Rosi and Sbrana, 1987) as well as on 1 syenitic ejecta samples found in the c.a 40 ka old
71 marker horizon known as Breccia Museo (BM) deposit (Gebauer et al., 2014).

72 **ANALYTICAL METHODS AND RESULTS**

73 Details on studied materials and methods, as well as pertinent tables (Tables DR1, DR2
74 and DR3), are reported in the GSA Data Repository[1].

75 The analyzed rock samples consist of trachytic tuffs and latitic-trachytic lavas with
76 primary phenocrysts of sanidine, clinopyroxene, biotite, magnetite, plagioclase and apatite (in
77 trace) (Tables DR1, DR2). The hydrothermal paragenesis exhibits a distribution that reflects
78 depth - temperature of the cored rocks (Tables DR1, DR3). Low temperature minerals, such as
79 zeolites and clay minerals, characterize the upper region of the wells (argillic zone, De Vivo et
80 al., 1989); moderate temperature minerals such as illite/sericite, calcite, chlorite and albite
81 prevail until 230 °C (Mofete 5 well) to 240 °C (Licola 1) (chlorite-illite zone, De Vivo et al.,
82 1989) and are joined at greater depth and temperature (until c.a 300 °C; Mofete 5 and San Vito
83 1) by pyrite and quartz; higher- temperature mineralogical assemblages (with abundant epidote,
84 zircon, scapolite, calcite and siderite: calcium-aluminum zone, De Vivo et al., 1989) are
85 dominant in the deepest and hottest levels. Such temperature distribution of hydrothermal
86 minerals is comparable to that reported for other fossil and active geothermal fields (Browne,
87 1978).

88 Stable isotope compositions of hydrothermal calcite and its concentration were measured
89 at INGV-OV Naples, Italy, by using a Spectrometer Finnigan Mat Delta plus. Calcite was found
90 in all core samples with concentration ($C_{calcite}$) varying from 0.045 g kg^{-1} to 140 g kg^{-1}. No
91 systematic dependence of $C_{calcite}$ on well depth/temperature was observed. The $\delta^{13}C$ (vs PDB)

92 and $\delta^{18}O$ (vs SMOW) ranged from –4.5‰ to 0.5‰ and from +7.5‰ to +19.3‰ respectively
93 (Table DR1). Hydrothermal mineral chemistry was determined using a JEOL-JXA-8200 electron
94 microprobe (WD/ED combined micro analyzer) (INGV Rome, Italy).

95 **DISCUSSION**

96 **Origin of the Water Precipitating Hydrothermal Calcite**

97 Oxygen isotope data constrain the oxygen isotopic composition of the hydrothermal
98 solutions ($\delta^{18}O_{H2O}$) associated with calcite formation (Simmons and Christenson, 1994).
99 Calculations were performed using the calcite-water fractionation factors of Friedman and
100 O'Neil (1977) at the pertinent well temperatures (Table DR1).

101 The computed $\delta^{18}O_{H2O}$ values range in a wide interval, from –3.5‰ to +13.8‰, and
102 positively correlate with sampling depth (Fig. 2): the shallowest samples, i.e., those of the
103 CFDDP well (depths of respectively 446 m and 506 m), exhibit the most negative $\delta^{18}O_{H2O}$
104 values, i.e., the closest to the local meteoric water (~–6.5‰); while the deepest samples,
105 including BM (for which a mineral paragenesis temperature of ~700 °C was estimated by
106 Gebauer et al., 2014), show the most positive values. Importantly, these "deep" calcites have
107 $\delta^{18}O_{H2O}$ of +8.7‰ to +12.7 ‰, i.e., in the typical range of magmatic water in subduction zones
108 (+8‰ to +12 ‰ Giggenbach, 1992). At CF, in particular, a $\delta^{18}O$ of ~+9‰ was inferred for the
109 magmatic water based on the fumarolic gas record (Chiodini et al., 2010).

110 Information on the salinity of solutions involved in hydrothermal mineralization at CF is
111 available from fluid inclusions trapped in k-feldspar, quartz and calcite (De Vivo et al., 1989).
112 The fluid inclusions that correspond to well-depths of our core samples are highlighted in Figure
113 2 as empty or gray circles: the empty circles refer to low-moderate salinities (2–6 wt.% NaCl
114 equivalent), and the gray circles to high salinities (26–49 wt.% NaCl equivalent). Interestingly,

low salinity solutions correspond to levels where calcites are isotopically lighter ($\delta^{18}O_{H2O}$ from +1.5‰ to +2.6‰), while high salinity solutions correlate with heavy oxygen isotopic compositions (from +11.5‰ to +12.7‰). This correlation supports a magmatic origin for both the hypersaline fluids reported by De Vivo et al. (1989) and the ^{18}O-rich calcite-precipitating solutions. According to Fournier (1999), brines and steam exsolved from crystallizing magma accumulate at high temperatures (> 400 °C) and lithostatic pressures in thin horizontal lenses in the plastic zone, from which they are episodically injected into the overlying brittle domain of meteoric-derived circulating fluids. We argue that, at CF, deep magmatic brines may have entered the shallow hydrothermal system during past magma degassing episodes, similar to those associated with recent (post 1982) bradyseismic events (Chiodini et al., 2012; 2015).

Although the ensemble of the possible processes controlling the oxygen isotopic composition of hydrothermal solutions is complex, including, for example, high-temperature water-rock-interactions (that concur to shift $\delta^{18}O_{H2O}$ toward more positive compositions), our results overall depict a mixing model (Fig. 2) between magmatic and shallow fluid components, either meteoric or marine, that is reminiscent of the mixing relations established based upon stable isotope compositions of present-day CF fumaroles (Chiodini et al., 2010).

Origin of Carbon Stored in the CF Hydrothermal Calcites

The source of carbon in CF calcites is investigated using the method proposed by Simmons and Christenson (1994) for the Broadlands geothermal system. The method involves comparing analytical data (well temperatures and $\delta^{13}C_{calcite}$ compositions) from the target hydrothermal system with the theoretical fractionation curves expected at CO_2-calcite isotopic equilibrium. The theoretical curves were calculated for a range of $CO_{2\ gas}$ isotopic compositions and temperatures (Fig. 3a) using the fractionation factors of Bottinga (1968). Figure 3a shows for

138 comparison the Broadlands results, in which calcites are thought to have equilibrated with a
139 $CO_{2,gas}$ isotopically similar to the magmatic influx ($\delta^{13}C$ ~–7.5‰) into the present-day
140 geothermal system (Simmons and Christenson, 1994).

141 The CF results are compositionally distinct from the Broadlands data set, and support an
142 isotopically heavier signature for the source CO_2, close to that currently discharged at SP
143 fumaroles ($\delta^{13}C$ = –1.3‰ ± 0.4; Chiodini et al., 2010). In Figure 3b, the carbon isotopic
144 compositions of equilibrium CO_2 gas ($\delta^{13}C_{CO2}$), which are computed by using pertinent
145 fractionation factors (Friedman and O'Neil, 1977) at the in situ temperature, are plotted against
146 depth. The diagram suggests that the light $\delta^{13}C_{CO2}$ compositions, derived from CFDDP samples,
147 possibly reflect infiltration, in the shallowest part of the caldera succession, of shallow
148 groundwaters transporting organic-derived carbon dissolved by recharge meteoric waters as they
149 infiltrate through soils. Apart from these shallow samples, Figure 3b strongly suggests that a
150 single, stable source of CO_2, the same that currently feeds the fumarolic field of SP, has been
151 involved in the past deposition history of CF hydrothermal calcites. The oldest pre-Campanian
152 Ignimbrite products (BM) of our data set indicate a $\delta^{13}C_{CO2}$ of ~–1.5‰, virtually identical to the
153 current fumarolic composition.

154 **The CF Carbon Budget Revealed by Hydrothermal Calcites**

155 The CO_2 that reacted with the host rocks of the CF hydrothermal system is stored in
156 equivalent amounts of hydrothermal calcite. A lower range estimate for the magmatic CO_2
157 associated to the entire CF history (~ 40 ka) can therefore be obtained by the mass of deposited
158 calcites. This is given by the product of $C_{calcite}$ by the volume of rocks affected by deposition of
159 hydrothermal calcite (V_{hc}), scaled to an average rock density of ~ 2.4 ton m^{-3} (De Vivo et al,
160 1989). By using a graphical method based on log plots (see footnote 1), we estimated a mean

$C_{calcite}$ of 25.7 g kg^{-1} (90% confidence interval, 13.2-45.6 g kg^{-1}). V_{hc} is estimated as the volume of a cylinder with 12-14 km diameter (extension of the caldera) and height of 2.5 km (depth to which calcites were actually observed) to 4 km (top of the CF shallower magma chamber). Using these numbers, we calculate a total mass of "calcite-stored" magmatic CO_2 of 12 Gt (90% confidence interval, 6-22 Gt). If normalized to a depositional interval of ~40 ka, this mass would covert into a time-averaged CO_2 flux of ~800 t d^{-1}. This "geological" CO_2 flux is of the same order of magnitude of the CO_2 currently released by diffuse degassing processes at SP (1100 ± 200 t d^{-1} in the 1998–2008 period, Chiodini et al., 2010), and falls within the typical range of present-day CO_2 fluxes from active calderas of the world (Table DR4).

We caution that our calculated flux here should be viewed as order of magnitude estimate only. In order to reduce the uncertainties associated with our inferred CO_2 flux, more observations would be needed to better constrain $C_{calcite}$ (which is currently based upon a relatively low number of measurements) and V_{hc}. We argue, however, that our presently estimated $C_{calcite}$ derives from randomly selected cores samples, and that a large depositional volume (V_{hc}) is supported by hydrothermal calcite being identified, even not quantified, in nearly all the analyzed core samples (De Vivo et al., 1989; Rosi and Sbrana, 1987), including those located in opposite sites of the caldera (i.e. L1 and CFDDP, where $C_{calcite}$ was qualitatively estimated at 50-200 g kg^{-1}; Mormone et al., 2015).

GENERAL IMPLICATIONS AND CONCLUDING REMARKS

Our novel results on hydrothermal calcites, presented here, demonstrate that a sizeable (~800 t d^{-1}) magmatic CO_2 release has persisted throughout the entire CF history. Because processes of natural CO_2 sequestration are widespread at hydrothermal systems, we conclude that calcite-stored CO_2 may represent a significant fraction of the CO_2 budget of calderas, that

184 has remained unaccounted for in previous volatile inventories. The sparse measurements that are
185 currently available (Table DR4) demonstrate a cumulative CO_2 emission from the few (n = 19)
186 "measured" calderas of ~21 Mt/yr, or 4-30% of the estimated global volcanic sub-aerial CO_2 flux
187 (Burton et al., 2013). Considering that calcite deposition has likely occurred at most of the 400
188 identified calderas, 97 of which were active in the Holocene (Newhall and Dzurisin, 1988), we
189 conclude that caldera-related CO_2 emissions can contribute, over geological timescales, a far
190 more substantial fraction of the global volcanic CO_2 flux than currently thought.

191 On a more local scale, the estimated "geological" CO_2 flux contributes to our
192 understanding of the geological evolution of the CF volcanic system, allowing for an estimate of
193 the (minimum) volume of parental (primitive) melts that have fed volcanic activity in the past. In
194 the Phlegraean volcanic District (Campi Flegrei, Ischia and Procida), the most-primitive (MgO
195 of ~6–7 wt%) and CO_2-rich (~2000–4000 ppm; Mormone et al., 2011; Moretti et al., 2013) melt
196 inclusions have been found trapped in mafic phenocrysts (olivine and cpx) of poorly evolved
197 magmas (shoshonites, trachybasalts) of Ischia and Procida; trachybasalts erupted at CF have
198 typically been more evolved and CO_2-depleted (Mangiacapra et al., 2008). Assuming the most
199 primitive compositions of Ischia and Procida as representative of the CF deep feeding system,
200 our stored CO_2 mass of ~12 Gt requires degassing of 1000–2000 km^3 of parental magma, with an
201 average magma feeding rate of 0.025–0.05 km^3/yr during the last 40 ka of activity. This
202 relatively large volume of degassing parental magma roughly agrees with the conclusions of
203 D'Antonio (2011) who claimed for 2500 km^3 of parent shoshonites as the source of erupted CF
204 magmas.

205 Finally, our observations here offer new lines of evidence to interpret the ongoing
206 degassing crisis of the CF caldera. The unrest has recently been interpreted as driven, at least

partially, by heating of hydrothermal host rocks, caused by an augmented injection of magmatic fluids into the hydrothermal system and a parallel compositional variation (more hydrous nature) of these fluids (Chiodini et al., 2015). As the hydrothermal system warms up, part of the past deposited calcite can become re-converted into CO_2 by reactions involving hydrothermal Ca-Al-silicates, contributing at least part of the present-day surface CO_2 emissions. Decarbonation of hydrothermal calcite must therefore be accounted for, as a potential CO_2 source, for a proper interpretation of gas monitoring time-series.

ACKNOWLEDGMENTS

The authors thank the Editor, E. Füri, S. Hurwitz, and T. Fischer for their insightful comments. This research was supported by a grant from European Research Council (ERC GA n. 305377) and the MEDiterranean SUpersite Volcanoes FP7 project (n. 308665). This work was inspired by discussion within the DECADE-DCO research initiative.

REFERENCES CITED

Bottinga, Y., 1968, Calculation of fractionation factors for carbon and oxygen exchange in the system calcite–carbon dioxide–water: The Journal of Chemical Physics, v. 72, p. 800–808, doi:10.1021/j100849a008.

Browne, P.R.L., 1978, Hydrothermal alteration in active geothermal systems: Annual Review of Earth and Planetary Sciences, v. 6, p. 229–248, doi:10.1146/annurev.ea.06.050178.001305.

Burton, M.R., Sawyer, G.M., and Granieri, D., 2013, Deep Carbon Emissions from Volcanoes: Reviews in Mineralogy and Geochemistry, v. 75, p. 323–354, doi:10.2138/rmg.2013.75.11.

Caprarelli, G., Tsutsumi, M., and Turi, B., 1997, Chemical and isotopic signatures of the basement rocks from the Campi Flegrei geothermal field (Naples, southern Italy): Inferences

about the origin and evolution of its hydrothermal fluids: Journal of Volcanology and Geothermal Research, v. 76, p. 63–82, doi:10.1016/S0377-0273(96)00072-8.

Chiodini, G., Caliro, S., Cardellini, C., Granieri, D., Avino, R., Baldini, A., Donnini, M., and Minopoli, C., 2010, Long-term variations of the Campi Flegrei, Italy, volcanic system as revealed by the monitoring of hydro-thermal activity: Journal of Geophysical Research, v. 115, p. B03205, doi:10.1029/2008JB006258.

Chiodini, G., Caliro, S., De Martino, P., Avino, R., and Gherardi, F., 2012, Early signals of new volcanic unrest at Campi Flegrei caldera? Insights from geochemical data and physical simulations: Geology, v. 40, p. 943–946, doi:10.1130/G33251.1.

Chiodini, G., Vandemeulebrouck, J., Caliro, S., D'Auria, L., De Martino, P., Mangiacapra, A., and Petrillo, Z., 2015, Evidence of thermal driven processes triggering the 2005–2014 unrest at Campi Flegrei caldera: Earth and Planetary Science Letters, v. 414, p. 58–67, doi:10.1016/j.epsl.2015.01.012.

D'Antonio, M., 2011, Lithology of the basement underlying the Campi Flegrei caldera: Volcanological and petrological constraints: Journal of Volcanology and Geothermal Research, v. 200, p. 91–98, doi:10.1016/j.jvolgeores.2010.12.006.

Del Gaudio, C., Aquino, I., Ricciardi, G.P., Ricco, C., and Scandone, R., 2010, Unrest episodes at Campi Flegrei: A reconstruction of vertical ground movements during 1905–2009: Journal of Volcanology and Geothermal Research, v. 195, p. 48–56, doi:10.1016/j.jvolgeores.2010.05.014.

De Vivo, B., Belkin, H.E., Barbieri, M., Chelini, W., Lattanzi, P., Lima, A., and Tolomeo, L., 1989, The Campi Flegrei (Italy) geothermal system: A fluid inclusion study of the Mofete

and San Vito fields: Journal of Volcanology and Geothermal Research, v. 36, p. 303–326, doi:10.1016/0377-0273(89)90076-0.

Fournier, R.O., 1999, Hydrothermal processes related to movement of fluid from plastic into brittle rock in the magmatic- epithermal environment: Economic Geology and the Bulletin of the Society of Economic Geologists, v. 94, p. 1193–1211, doi:10.2113/gsecongeo.94.8.1193.

Friedman, I., and O'Neil, J.R., 1977, Compilation of stable isotope fractionation factors of geochemical interest [KK.]: U.S. Geological Survey Professional Paper, v. 440, 11 p.

Gebauer, S.K., Schmitt, A.K., Pappalardo, L., Stockli, D.F., and Lovera, O.M., 2014, Crystallization and eruption ages of Breccia Museo (Campi Flegrei caldera, Italy) plutonic clasts and their relation to the Campanian ignimbrite: Contributions to Mineralogy and Petrology, v. 167, no. 1, p. 1–18, doi:10.1007/s00410-013-0953-7.

Giggenbach, W.F., 1992, Isotopic shifts in waters from geothermal and volcanic systems along convergent plate boundaries and their origin: Earth and Planetary Science Letters, v. 113, p. 495–510, doi:10.1016/0012-821X(92)90127-H.

Giggenbach, W.F., 1984, Mass transfer in hydrothermal alteration systems – A conceptual approach: Geochimica et Cosmochimica Acta, v. 48, p. 2693–2711, doi:10.1016/0016-7037(84)90317-X.

Hurwitz, S., and Lowenstern, J.B., 2014, Dynamics of the Yellowstone Hydrothermal System: Reviews of Geophysics, v. 51, doi:10.1002/2014RG000452.

Mangiacapra, A., Moretti, R., Rutherford, M., Civetta, L., Orsi, G., and Papale, P., 2008, The deep magmatic system of the Campi Flegrei caldera (Italy): Geophysical Research Letters, v. 35, no. 21, p. L21304, doi:10.1029/2008GL035550.

Moretti, R., Arienzo, I., Orsi, G., Civetta, L., and D'Antonio, M., 2013, The Deep Plumbing System of Ischia: A Physico-chemical Window on the Fluid-saturated and CO_2-sustained Neapolitan Volcanism (Southern Italy): Journal of Petrology, doi:10.1093/petrology/egt002.

Mormone, A., Piochi, M., Bellatreccia, F., De Astis, G., Moretti, R., Della Ventura, G., Cavallo, A., and Mangiacapra, A., 2011, CO_2-rich magma source beneath the Phlegraen Volcanic District (Southern Italy): Evidence from a melt inclusion study: Chemical Geology, v. 287, p. 66–80, doi:10.1016/j.chemgeo.2011.05.019.

Mormone, A., Troise, C., Piochi, M., Balassone, G., Joachimski, M., and De Natale, G., 2015, Mineralogical, geochemical and isotopic features of tuffs from the CFDDP drill hole: Hydrothermal activity in the eastern side of the Campi Flegrei volcano (southern Italy): Journal of Volcanology and Geothermal Research, v. 290, p. 39–52, doi:10.1016/j.jvolgeores.2014.12.003.

Newhall, C.G., and Dzurisin, D., 1988, Historical unrest at large calderas of the world: U.S. Geological Survey Bulletin 1855, 1108 p.

Pappalardo, L., and Mastrolorenzo, G., 2012, Rapid differentiation in sill- like magma reservoir: A case study from the campi flegrei caldera: Scientific Reports, v. 2, no. 712, doi:10.1038/srep00712.

Pappalardo, L., Ottolini, L., and Mastrolorenzo, G., 2008, The Campanian Ignimbrite (Southern Italy) geochemical zoning: Insight on the generation of a super-eruption from catastrophic differentiation and fast withdrawal: Contributions to Mineralogy and Petrology, v. 156, p. 1–26, doi:10.1007/s00410-007-0270-0.

Rosi, M., and Sbrana, A., 1987, Phlegrean Fields: CNR, Quaderni Ricerca Scientifica, v. 114, 175 p.

297 Simmons, S.F., and Christenson, B.W., 1994, Origins of calcite in a boiling geothermal system:
298 American Journal of Science, v. 294, p. 361–400, doi:10.2475/ajs.294.3.361.
299 Sparks, R.S.J., Self, S., Grattan, J.P., Oppenheimer, C., Pyle, D.M., and Rymer, H., 2005, Super-
300 eruptions: Global effects and future threats: Report of a Geological Society of London
301 Working Group, The Geological Society of London, 24 p.
302 Symonds, R.T., and Gerlach, M.R., 2001, Magmatic gas scrubbing: implications for volcano
303 monitoring: Journal of Volcanology and Geothermal Research, v. 108, p. 303–341,
304 doi:10.1016/S0377-0273(00)00292-4.
305 Zollo, A., Maercklin, N., Vassallo, M., Dello Iacono, D., Virieux, J., and Gasparini, P., 2008,
306 Seismic reflections reveal a massive melt layer feeding Campi Flegrei caldera: Geophysical
307 Research Letters, v. 35, p. L12306, doi:10.1029/2008GL034242.

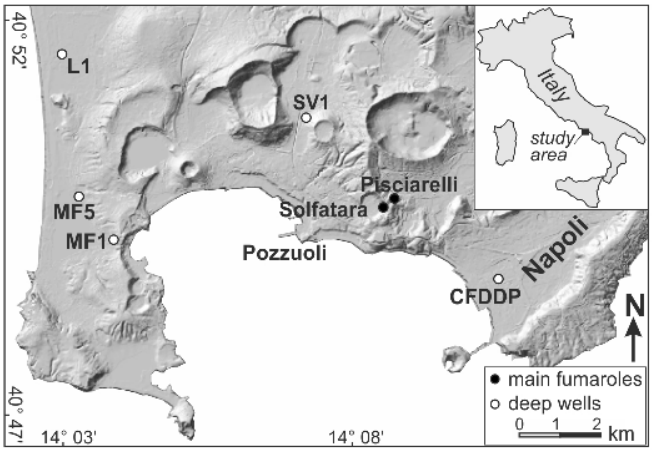

308

309 Figure 1. Shaded relief map of CF caldera with location of the studied deep wells L1 (Licola 1),

310 MF5 (Mofete 5), MF1 (Mofete 1, data from Caprarelli et al., 1997), SV1 (San Vito 1), CFDDP

311 (data from Mormone et al., 2015).

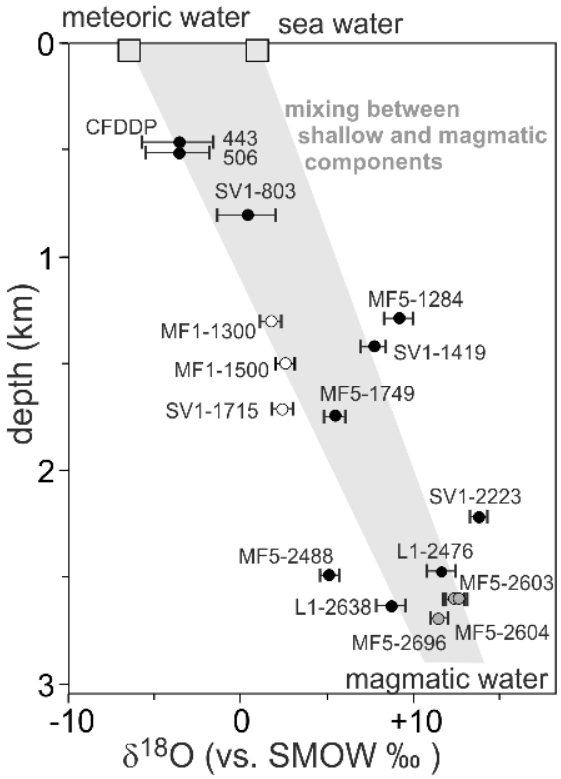

Figure 2. Oxygen isotopic composition of solutions precipitating calcite vs the sample depth. The first 3 characters of the sample labels refer to the well (see Fig. 1) while the last characters refer to sample depth. Empty and gray symbols refer respectively to low salinity and high salinity solutions (see text). Error bars express uncertainty in equilibrium temperatures (estimated at ± 20°C from homogenization temperatures of fluid inclusions; De Vivo et al. 1989).

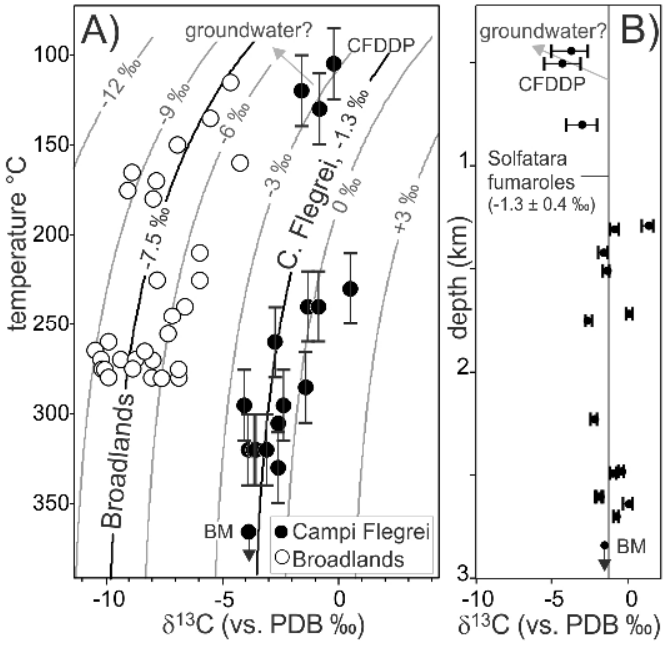

322

323 Figure 3. A) $\delta^{13}C_{calcite}$ vs temperature. Data of CF and of Broadlands (Simmons and Christenson,
324 1994) are compared to the theoretical values computed for original CO_2 (gas) of different
325 isotopic compositions (see text); B) carbon isotopic compositions of equilibrium CO_2 gas (CF) is
326 plotted against depth. See Fig. 2 for explanation of error bars.

Supplementary information for

The geological CO_2 degassing history of a long-lived caldera

Giovanni Chiodini[1], L. Pappalardo[2], A. Aiuppa[3], and S. Caliro[2]

[1]*INGV, Sezione di Bologna, via Creti 12, 40128 Bologna, Italy*

[2]*INGV, Sezione di Napoli, via Diocleziano 328, 80124 Napoli, Italy*

[3]*2Dipartimento CFTA, Università di Palermo, Via Archirafi 36, 90123 Palermo, Italy*

MATERIALS AND METHODS

The data obtained in this research refer to rock samples from three deep geothermal boreholes drilled by Agip in the caldera area (Mofete5, Licola1 and S. Vito1 wells) as well as plutonic syenitic clasts included in the Breccia Museo deposit.

Stable isotope compositions of carbon and oxygen on hydrothermal calcite and its concentration have been determined at Istituto Nazionale di Geofisica e Vulcanologia in Naples on powder samples by using a Spectrometer Finnigan Mat Delta plus. The accuracy of the measurements is ± 0.15 ‰ for $d^{13} C_{CO2}$, ± 0.1 ‰ for d^{18} O, and ± 10% for calcite concentration ($C_{calcite}$) (Table DR1). The CF data set was completed with previous published oxygen and carbon calcite compositions of Mofete 1 well (M1-1302 and M1-1500, Caprarelli et al., 1997) and of CFDDP (CFDDP-443 and CFDDP-506, Mormone et al., 2015) (Table DR1).

Polished thin sections of rock samples were analyzed by: (i) polarized light microscopy for a preliminary identification of the mineralogical assemblage, (Table DR1) and (ii) by electron microprobe (EMPA) for measurements of major element compositions of hydrothermal minerals, performed at Istituto Nazionale di Geofisica e Vulcanologia in Rome with a JEOL-JXA-8200 electron microprobe (WD/ED combined micro analyzer) using 15 kV voltage, a 10 mm beam spot and 10 nA beam current. The analytical uncertainty was about 1% for most elements. Results are reported in Table DR2.

STRATIGRAPHIC DESCRIPTION AND PETROGRAPHY OF STUDIED ROCKS

Samples were collected at different depths of three geothermal boreholes drilled in the proximity of the western border (Mofete5 and Licola1 wells) as well as in the central sector (S. Vito1 well) of the caldera, Figure DR1 (Agip, 1987, Rosi and Sbrana, 1987). In the western border of the caldera (Mofete 5 and Licola 1 wells) the cored stratigraphic succession is represented by pyroclastic rocks of post-caldera period, that buried a sequence of sedimentary submarine rocks inter-bedded with tuffs, tuffites and lava bodies. On the contrary, S. Vito 1 well, in the central sector of the caldera, has encountered prevalently the volcanic tuffs filling the calderic depression. Particularly, under a 500 meter thick pyroclastic succession of post-caldera age, two main volcanic tuff formations have been penetrated: a yellow tuff between 500 and 1000 m of depth and a gray tuff between 1000 and 2000 m of depth, probably emplaced during the two large-scale eruptions of the Neapolitan Yellow Tuff (14 ka) and of the Campanian Ignimbrite (40 ka), respectively.

The stratigraphy and the temperature profiles of the boreholes are shown in Figure DR1 with the sample locations. The sample name represents the specific well followed by the depth at which the sample was taken (i.e. M5 1284, Mofete 5 well, 1284 m of depth) while Breccia Museo ejecta are from two sites: Acquamorta at Monte di Procida, (samples: BM S-5-1, S-5-2,) and Punta della Lingua on Procida Island (samples BM S-1, S-2, S-3, S-4). Moreover, the distributions of mineral phases as a fuction of the temperature measured in the wells is reported in Table DR3.

Mofete 5 well. : The sample M5 1284 is a porphyritic lava with phenocrysts of feldspar and magnetite included in microcrystalline groundmass, secondary minerals of calcite, sericite and chlorite are widespread in the whole-rocks. The sample M5 1749 is a volcanic tuff, constituted by phenocrysts of feldspar and subordinately apatite dispersed in matrix glass, secondary minerals of calcite, sericite and chlorite are present in the matrix. The sample M5 2603 is an intrusive syenite constituted by primary minerals of feldspars, and secondary of calcite, quartz, siderite, epidote, zircon and scapolite. The samples M5 2488 and M5 2696 belong to a deep volcanic tuffites characterized by fine-grained cineritic matrix in which are widespread polygenic lithic clasts and

scoriae. Phenocrysts are represented by euhedral and subeuhedral alkali feldspar, biotite, magnetite, and clinopyroxene. Calcite is also present as well as epidote, pyrite, quartz, siderite, scapolite, sphene and amphibole.

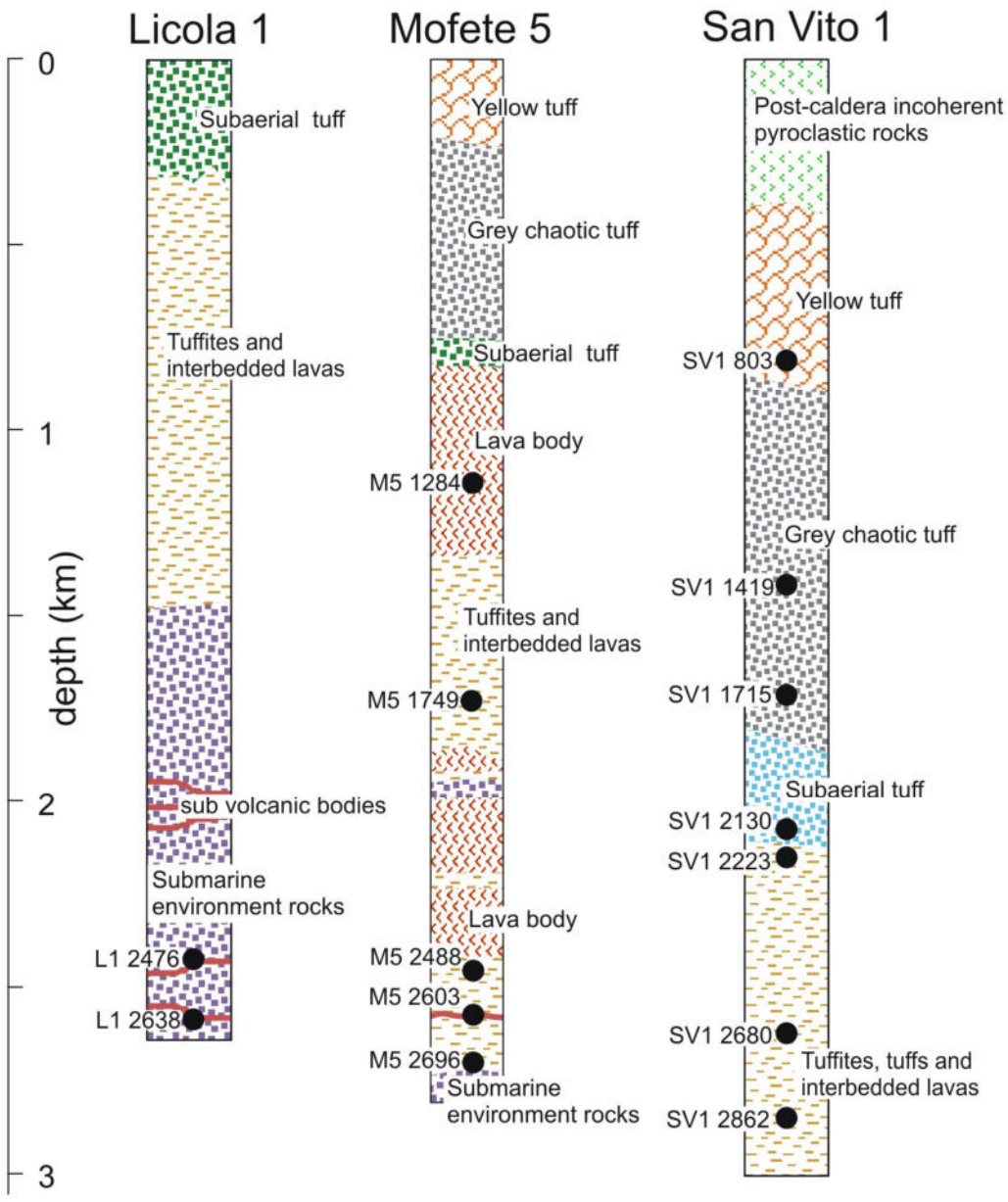

Figure DR1 – Lithostratigraphic sections of the studied geothermal boreholes.

Licola1 well : The samples L1 2476, is a porphyritic lava with phenocrysts of plagioclase and alkali feldspar, with advanced sericite-type alteration process, albite, calcite and pyrite are also present. The sample L1 2638 is a deep lava body constituted by phenocrysts of feldspars, biotite,

magnetite and apatite and secondary minerals of albite, calcite, chlorite, sericite, perovskite, fluorite, zircon.

S. Vito 1: Sample SV1 803 belongs to the Neapolitan Yellow Tuff formation and consists phenocrysts of k-feldspar, magnetite and cpx. Secondary minerals include sodalite, sericite, calcite. The samples SV1 1419 and SV1 1715 are part of the Campanian Gray tuff. They are constituted by euedral phenocrysts of sanidine, plagioclase, clinopyroxene, magnetite, biotite and apatite distributed in an abundant altered matrix-glass. Secondary minerals include sericite, calcite, chlorite, albite and zeolite. Below the Campanian gray tuff, pre-calderic rocks are formed by the alternation of volcanic tuffs, lavas and tuffites. The sample SV1 2130 is constituted by a gray tuff formed predominantly by phenocrysts of plagioclase included in an altered matrix glass with abundant secondary minerals of calcite, chlorite, pyrite and quartz; while the sample SV1 2862 belongs to a deeper volcanic tuff formed by phenocrysts of plagioclase, clinopyroxene, magnetite and secondary minerals of sericite, calcite, pyrite, epidote. Reworked levels (SV1 2223 and 2680) are intercalated between the latter pre-calderic tuffs. In these deep samples the primary structure is no longer recognizable, while predominate secondary minerals of sericite, calcite, chlorite, pyrite, quartz, amphibole, epidote.

Syenitic plutonic clasts: The syenitic clasts are consitituted prevalently by subhedral to anhedral potassium feldspar (70%) and plagioclase (20%). Cancrinite (hauyna) was identified as a minor component in some samples. Mafic mineral assemblages are constituted by clinopyroxene and biotite often intergrown with chlorite. Hornblende is often present as an overgrowth over relict clinopyroxene. Accessory minerals are zircon and sphene, apatite, opaques (ilmenite), garnet, scapolite, fluorite, pistacite.

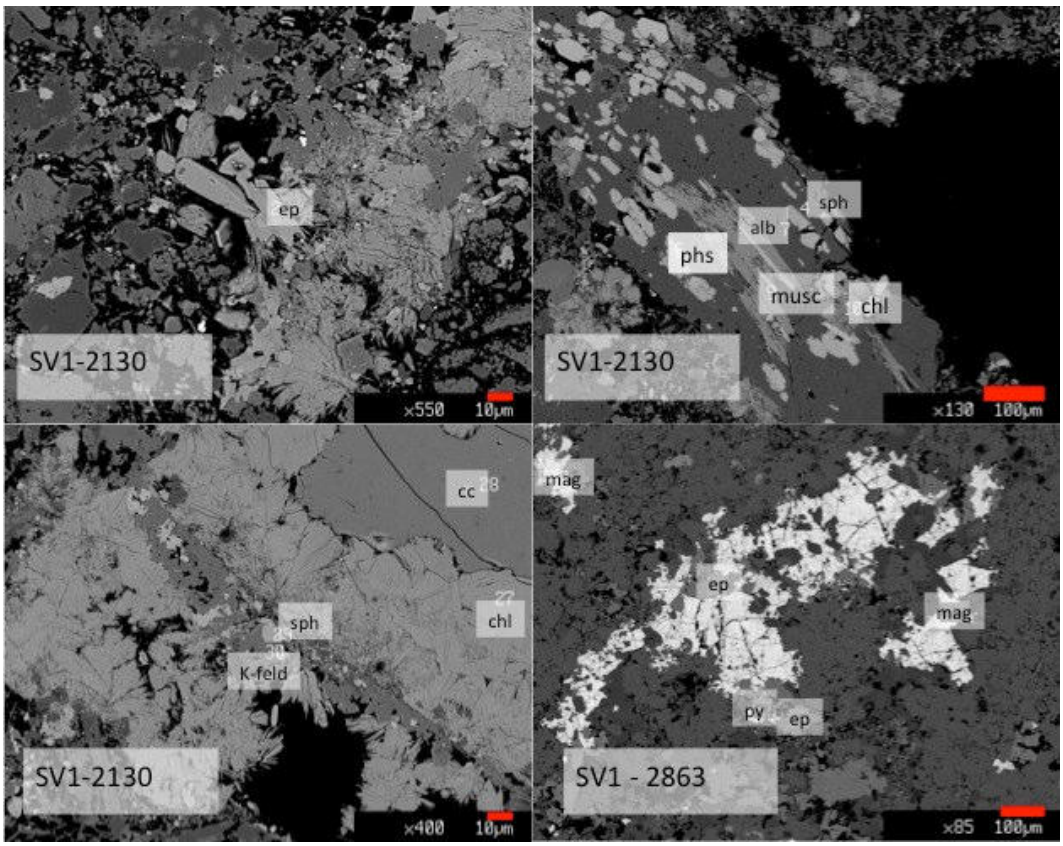

Figure DR2 A) –Examples of back-scattered electron images of polished thin sections representative of samples from studied wells.

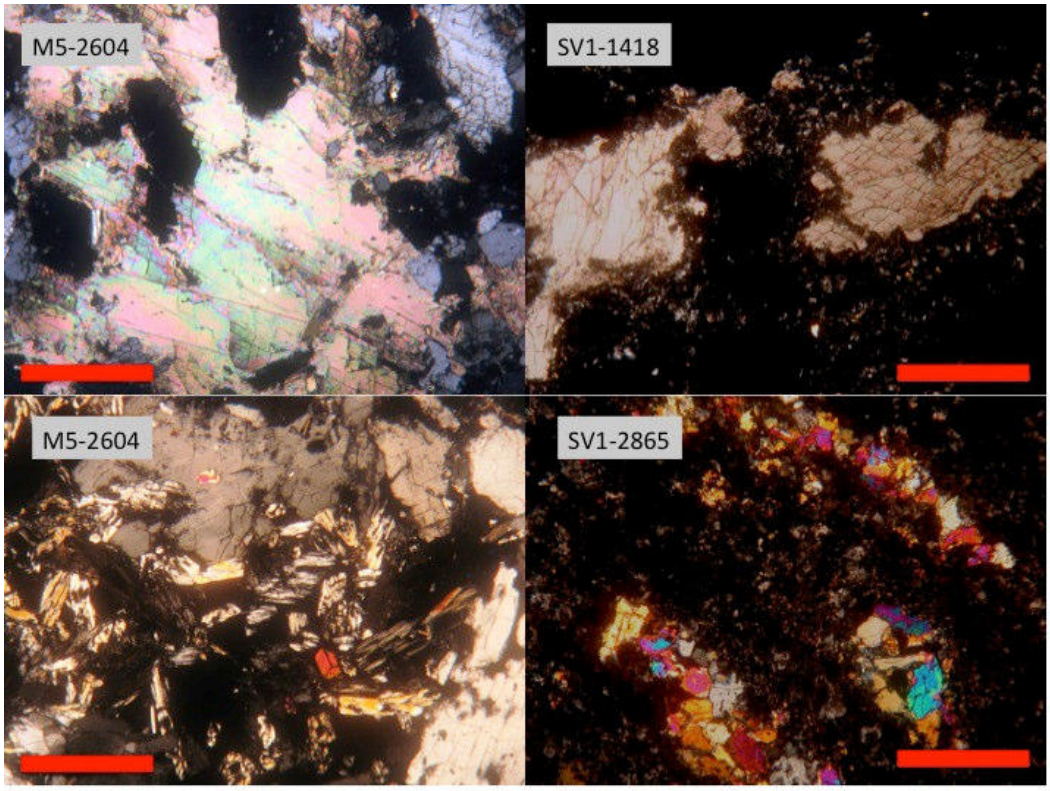

Figure DR2 B) Examples of photomicrographs of thin sections of samples from studied wells. Scale bars represent 1000 µm. Upper images: calcite crystals, cross-polarized light; lower images: epidote crystals, cross-polarized light.

COMPUTATION OF THE AVERAGE CALCITE CONCENTRATION

The $C_{calcite}$ dataset of core samples (i.e. excluding the Breccia Museo sample) define, in a log-probability plot (Supplementary Figure 3), a curve with an inflection point that we interpret as due to the presence of two overlapping log-normal populations. Applying the graphic method of Sinclair (1974), the original dataset can be partitioned into two log-normal populations, with respectively high (Population A, 70%) and low (Population B, 30%) $C_{calcite}$ values.

.

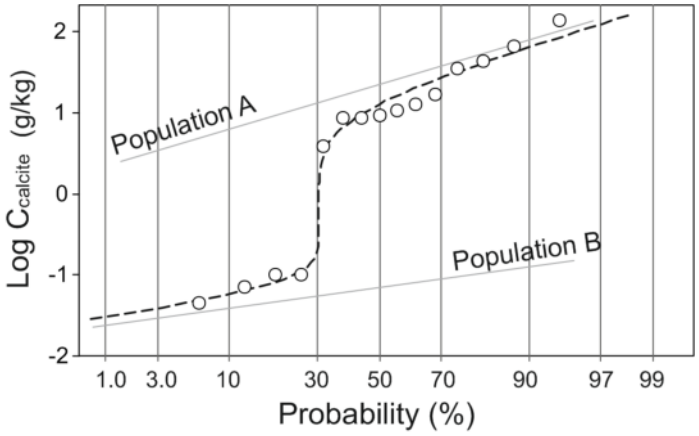

Figure DR3 – Probability plot of $C_{calcite}$ and partitioning of the data in the two log-normal populations A and B.

We used a Montecarlo procedure to estimate the mean $C_{calcite}$ values, M_i (and their 90% confidence intervals), for both populations; these resulted $M_B = 0.08$ g kg^{-1} (90% c.i from 0.052 g kg^{-1} to 0.113 g kg^{-1}) for population B, and $M_A = 36.7$ g kg^{-1} (90% c.i from 18.8 g kg^{-1} to 65.1 g kg^{-1}) for population A. Considering the fractions of the two populations we estimate an average $C_{calcite}$ of 25.7 g kg^{-1} (90% confidence interval from 13.2 g kg^{-1} to 45.6 g kg^{-1})

TABLE DR1. PARAGENESIS AND CHEMICAL-ISOTOPIC COMPOSITION OF THE ANALYZED ROCKS

	lithology	**T** (°C)	**primary minerals**	**hydrothermal minerals**	C_{CaCO3} (g / Kg)	$^{13}C_{calcite}$ (d‰)	$^{18}O_{calcite}$ (d‰)
SV1 803	tuff	130	k-fld, mt, cpx	sod, ms, cc, py	8.81	-0.86	14.68
SV1 1419	tuff	260	k-fld, pl, cpx, ap, ti-mt, bt	zeol, ms, cc, ab	12.9	-2.76	14.63
SV1 1715	tuff	285	k-fld, pl, cpx, ap, ti-mt, bt	ms, cc, chl	10.9	-1.42	8.49
SV1 2130	tuff	300	k-fld	ms ,cc, chl py, qz, ab	0.045	n.d.	n.d.
SV1 2223	reworked	320	not recognizable crystals	cc, chl py, qz, amp	8.63	-3.90	18.81
SV1 2680	reworked	350	not recognizable crystals	ms, cc, py, ep	0.10	n.d.	n.d.
SV1 2862	tuff	390	pl, cpx, mt	ms, cc, ep, py, ab	0.071	n.d.	n.d.
M5 1284	lava	230	pl, k-fld, ti-mt	ms, cc, ab, sph	3.87	0.47	17.28
M5 1749	tuff	295	pl, k-fld, ap	ms ,cc ,chl, ab, py	140	-4.08	11.23
M5 2488	reworked	305	k-fld	ms ,cc ,py, qz	0.10	-2.59	10.59
M5 2603	reworked	320	not recognizable crystals		35.3	-3.65	17.41
M5 2604	intrusive	320	pl, k-fld	cc, qz, sid, ep, zr, scap	9.41	-3.55	17.69
M5 2696	tuff	330	cpx, mt	cc, py, qz, sid, ep, scap, sph, amp	17.2	-2.62	16.25
L1 2476	lava	240	k-fld	ab, ser, cc, py	43.4	-1.33	19.37
L1 2638	lava	240	pl, k-fld,ti-mt,ap,bt	ab, ser, cc, py, chl, zeol, fl, pw	67.4	-0.90	16.40
BMS52	syenite		pl, k-fld, cpx, sph	zr, amp, cc	0.40	-3.88	12.37
*M1 1299-1306	lava	295	pl,k-fld,ap,mt,bt	cc, qz, ab, py, ep, ser, ms, chl		-2.4	7.60
*M1 1495-1503	tuffite	320	san,pl,cc,bt,ap	cc, qz ,ab,py,ep,ser, chl		-3.1	7.50
†CFDDP 443	tuff	105	k-fld, cpx, bt, mt, pl	alb,cc, py,qz, ms	50-200	-0.24	13.30
†CFDDP 506	tuff	120	k-fld, cpx, bt, mt, pl	alb,cc, py,qz, ms	50-200	-1.83	11.60

Note: Carbon isotopic composition are VS PDB and oxygen VS SMOW. Temperature by De Vivo et al., 1989.k-fld=K-feldspar, mt=magnetite, cpx=clinopyroxene, pl=plagioclase, ap=apatite, ti-mt=Ti-magnetite, bt=biotite, sod=sodalite, ms=sericite, cc=calcite., zeol=zeolite, chl=chlorite, py=pyrite, qz=quartz, amp=amphybole, ep=epidote, sid=siderite, scap=scapolite, sph=sphene, zr=zircon, ab=albite, fl=fluorite, pw=perowskite

* data from Caprarelli et al. (1997)

† data from Mormone et al. (2015). According to most recent measurements (Carlino et al., in preparation), obtained in more stabilised conditions, the well CFDDP temperatures are 40°C higher than reported in Mormone et al (2015).

TABLE DR2. SELECTED MICROPROBE ANALYSES OF MINERALS

samples	**L1-2476**	**L1-2476**	**L1-2635**	**L1-2635**	**L1-2635**	**L1-2635**
	albite	pyrite	muscovite	apatite	Ti-mt	k-feld
SiO_2	70.33	0.07	50.73	1.14	0.05	65.95
TiO_2	-	-	0.02	-	7.07	0.02
Al_2O_3	19.39	0.02	29.88	0.02	3.54	18.36
FeO	0.02	65.63	2.56	0.18	82.82	0.03
MnO	0.01	0.05	-	0.13	0.07	-
MgO	-	-	1.51	0.15	0.02	0.01
CaO	0.01	0.01	0.06	53.81	-	0.01
Na_2O	11.68	0.02	0.32	0.22	-	0.59
K_2O	0.04	0.02	9.49	0.02	-	15.15
P_2O_5	-	-	0.01	38.51	-	-
F	-	-	0.69	2.43	-	0.08
Cl	-	-	0.01	0.51	-	-
samples	**L1-2640/43**	**L1-2640/43**	**L1-2640/43**	**L1-2635**	**L1-2635**	**L1-2635**
	biotite	perovskite	fluorite	sphene	gypsium	calcite
SiO_2	48.92	3.09	0.13	30.33	-	-
TiO_2	0.11	48.54	-	33.46	0.03	-
Al_2O_3	30.12	0.77	0.07	4.77	0.06	-
FeO	2.34	1.09	0.03	1.00	0.03	-
MnO	0.00	0.57	-	0.06	0.02	0.33
MgO	1.78	0.26	-	0.00	0.03	-
CaO	0.01	25.05	76.98	28.39	39.87	60.46
Na_2O	0.09	0.05	0.00	0.06	-	0.00
K_2O	9.54	0.01	0.37	0.13	-	0.01
P_2O_5	0.01	0.03	-	0.04	-	-
F	0.65	0.46	44.33	1.63	0.26	0.12
Cl	0.04	0.03	-	0.02	0.01	-
S	-	-	-	-	51.75	-
samples	**L1-2636**	**M5-1749**	**M5-2604**	**M5-2604**	**M5-2604**	**M5-2695**
	chlorite	albite	quartz	siderite	scapolite	pyrite
SiO_2	27.84	66.04	101.96	-	56.72	0.02
TiO_2	0.03	0.04	-	-	0.01	-
Al_2O_3	19.05	20.08	0.01	-	22.09	0.02
FeO	24.14	0.06	0.66	63.56	0.02	47.42
MnO	0.59	0.00	0.00	-	0.02	0.05
MgO	16.04	0.00	0.01	-	0.02	-
CaO	0.13	1.07	0.00	-	7.01	0.02
Na_2O	0.05	6.49	0.01	-	9.51	-
K_2O	0.06	6.46	0.01	-	1.31	-
P_2O_5	-	0.01	0.03	0.05	0.01	-
F	0.34	-0.01	-	0.10	0.01	0.49
Cl	-	-	-	-	3.50	-
S	-	-	-	-	-	45.08

TABLE DR2. CONTINUED

samples	**M5-2695**	**M5-2695**	**SV1 -2222**	**SV1 -2222**	**SV1 -2222**	**SV1 -2222**
	epidote	sphene	quartz	amphibole	chlorite	pyrite
SiO_2	30.21	30.41	95.68	52.41	32.56	0.02
TiO_2	0.33	30.04	-	0.04	0.04	0.01
Al_2O_3	14.97	6.00	1.48	30.78	20.18	0.01
FeO	13.70	1.51	0.05	1.14	5.34	59.99
MnO	0.26	0.08	0.12	0.08	0.22	0.04
MgO	1.05	0.06	0.02	1.67	29.59	-
CaO	12.79	28.73	0.46	12.61	0.06	0.01
Na_2O	-	-	0.30	3.78	0.03	0.01
K_2O	0.01	-	0.26	0.62	0.74	0.01
P_2O_5	0.02	0.01	0.01	0.04	0.00	0.02
F	0.89	2.75	0.53	0.02	0.01	-
Cl	-	-	-	0.16	-	0.27
S	-	0.02	0.03	-	0.01	28.64
samples	**SV1-1714**	**SV1-1418**	**SV1-1418**	**SV1-2130**	**SV1-2130**	**SV1-2130**
	chlorite	calcite	albite	epidote	sericite	chlorite
SiO_2	28.38	0.01	69.24	36.94	36.54	27.77
TiO_2	-	0.01	-	0.20	4.87	-
Al_2O_3	17.93	0.01	20.98	21.53	14.97	16.35
FeO	28.12	0.08	0.04	14.38	13.84	30.73
MnO	2.81	0.46	-	0.36	0.17	1.31
MgO	12.92	-	0.01	0.05	15.98	12.79
CaO	0.08	52.07	0.60	22.35	0.08	0.22
Na_2O	0.04	-	11.25	-	0.32	-
K_2O	-	0.03	0.11	0.14	9.77	0.04
P_2O_5	0.01	-	-	-	-	0.02
F	-	-	-	0.24	-	-
Cl	-	0.36	0.19	-	0.08	0.02
S	-	-	0.04	0.06	0.02	-
samples	**SV1-2130**	**SV1-2130**	**SV1-2863**	**SV1-2863**	**SV1-2863**	**SV1-2863**
	sphene	albite	epidoto	pyrite	ms	albite
SiO_2	30.99	65.93	37.06	0.02	38.30	67.50
TiO_2	27.64	0.08	-	-	2.30	-
Al_2O_3	7.06	20.38	24.52	-	15.47	20.38
FeO	2.10	0.19	11.36	61.17	18.97	0.10
MnO	0.02	0.01	0.21	-	0.28	-
MgO	0.04	0.01	0.04	-	12.85	-
CaO	27.16	1.43	22.88	0.03	-	0.46
Na_2O	0.04	10.63	0.01	0.01	0.16	10.96
K_2O	0.18	0.14	-	0.02	9.85	0.32
P_2O_5	-	0.05	-	-	0.02	0.01
F	2.54	0.08	0.15	0.35	-	0.22
Cl	0.04	0.01	-	0.01	0.02	-
S	-	0.08	-	34.95	0.02	0.01

TABLE DR2. CONTINUED

samples	**BM-S52**	**BM-S52**	**BM-S52**	**BM-S52**	**BM-S51**	**BM-S51**
	mt5	fluorite	ilmenite	horneblende	scapolite	pistacite
SiO_2	0.05	0.04	0.01	40.68	59.12	36.60
TiO_2	2.54	-	51.76	2.76	-	0.42
Al_2O_3	0.74	-	0.02	11.05	20.51	5.92
FeO	87.37	0.04	38.88	15.69	0.19	20.10
MnO	2.25	0.02	10.22	0.98	-	4.78
MgO	0.22	-	0.74	10.61	0.03	0.08
CaO	0.04	72.86	0.02	11.48	4.26	29.92
Na_2O	0.02	0.01	0.03	2.42	11.02	0.03
K_2O	-	-	-	2.02	1.57	0.02
P_2O_5	-	-	-	-	0.03	0.01
Cl	0.01	0.02	-	0.10	3.78	-
F	-	43.68	-	1.57	0.01	0.01
S	-	-	-	0.05	-	-

samples	**BM-S51**	**BM-S51**	**BM-S4**	**BM-S4**	**BM-S4**	**BM-S4**
	epidote	fluorite	ulvospinel	sphene	sphene	Hauyna
SiO_2	31.02	0.04	0.06	29.58	29.85	32.19
TiO_2	0.63	0.01	2.63	31.24	30.69	0.03
Al_2O_3	13.98	-	0.87	2.96	2.88	27.39
FeO	14.33	0.10	86.21	2.77	2.88	0.21
MnO	0.99	-	2.07	0.20	0.16	-
MgO	0.22	-	0.32	0.17	0.14	-
CaO	13.87	72.15	0.08	27.39	26.62	10.07
Na_2O	-	0.02	0.10	-	0.02	13.86
K_2O	-	0.02	-	-	0.01	3.18
P_2O_5	-	-	-	0.01	0.03	-
Cl	-	0.02	0.01	0.01	0.00	7.15
F	0.14	45.62	0.00	1.57	1.63	0.01
S	-	-	0.25	-	-	4.41

TABLE DR3 - MINERAL ZONATION IN CORED SAMPLES AS A FUCTION OF TEMPERATURE

Calcite+Chlorite+illite zone			*Calcite+pyrite+quartz zone*		*Calcite+ epidote zone*		*Alteration zone*
SV1 803	**SV1 1419**	**SV1 1715**	**SV1 2130**	**SV1 2223**	**SV1 2680**	**SV1 2862**	*Mineralogy*
X							*sodalite*
	X						*zeolite*
	X		X			X	*albite*
X	X	X	X		X	X	*illite/sericite*
X	X	X	X	X	X	X	*calcite*
		X	X	X			*chlorite*
X			X	X	X	X	*pyrite*
			X	X			*quartz*
							siderite
			X		X	X	*epidote*
							zircon
							fluorite
							scapolite
							perovskite
			X				*sphene*
				X			*amphibole*
130	**260**	**285**	**300**	**320**	**350**	**390**	**T°C**

Calcite+Chlorite+illite zone			*Calcite+pyrite+quartz zone*		*Calcite+ epidote zone*		*Alteration zone*
L12476	**L12635**	**M5 1284**	**M5 1749**	**M5 2488**	**M5 2604**	**M5 2696**	*Mineralogy*
							sodalite
	X						*zeolite*
X	X	X	X				*albite*
X	X	X	X	X			*illite/sericite*
X	X	X	X	X	X	X	*calcite*
	X						*chlorite*
X			X	X		X	*pyrite*
				X	X	X	*quartz*
					X	X	*siderite*
					X	X	*epidote*
	X				X		*zircon*
	X						*fluorite*
					X	X	*scapolite*
	X						*perovskite*
		X				X	*sphene*
						X	*amphibole*
240	**240**	**230**	**295**	**305**	**320**	**330**	**T°C**

TABLE DR4. CO_2 FLUX FROM CALDERAS

Name	**State**	**feature**	**CO_2-Flux (ton/d)**	**Reference**
Pinatubo	Philippines	lake	884	Perez et al (2011)
Taal	Philippines	lake	739	Perez et al (2011)
Apoyeque	Nicaragua	lake	212	Perez et al (2011)
Apoyo	Nicaragua	lake	539	Perez et al (2011)
Jiloa	Nicaragua	lake	734	Perez et al (2011)
Masaya	Nicaragua	lake	869	Perez et al (2011)
Rotomahana	New Zeland	lake	549	Mazot et al. (2014)
Yellowstone	USA	diffuse soil emission	46000	Werner and Brantley (2003)
Mammoth-LongValley	USA	diffuse soil emission	552	Sorey et al. (1998)
Somma-Vesuvio	Italia	diffuse emission, groundwater	301	Caliro et al. (1995a)
Campi Flegrei	Italia	diffuse soil emission	1500	Chiodini et al. (2001)
Latera	Italia	diffuse soil emission	350	Chiodini et al. (2007)
Colli Albani	Italia	groundwater	500	Chiodini and Frondini (2001)
Furnas	Azzorre	diffuse soil emission	968	Viveiros et al. (2010)
Nisyros	Greece	diffuse soil emission	68	Caliro et al. (2005b)
Teide	Spain	diffuse soil emission	76	Perez et al. (2013)
Rotorua	New Zeland	diffuse soil emission	1000	Werner and Cardellini (2006)
Rotokawa	New Zeland	diffuse soil emission	440	Bloomberg et al. (2014)
El Chichon	Mexico	lake+diffuse soil emission	370	Mazot et al. (2011)

REFERENCES CITED

Agip, 1987, Geologia e geofisica del sistema geotermico dei Campi Flegrei: Unpublished Internal Report, 17 pp.

Bloomberg, S., Werner, C., Rissmann, C., Mazot, A., Horton, T., Gravley, D., Kennedy, B., and Oze, C. , 2014, Soil CO2 emissions as a proxy for heat and mass flow assessment, Taupo Volcanic Zone New Zealand: Geochemistry Geophysics Geosystems, v. 15, p. 4885–4904, doi:10.1002/2014GC005327.

Caliro, S., Chiodini, G., Avino, R., Cardellini, C., Frondini, F. , 2005, Volcanic degassing at Somma-Vesuvio (Italy) inferred by chemical and isotopic signatures of groundwater: Applied Geochemistry, v. 20 (6), p. 1060-1076.

Caliro, S., Chiodini, G., Galluzzo, D., Granieri, D., La Rocca, M., and Ventura G., 2005b, Recent activity of Nisyros volcano (Greece) inferred from structural, geochemical and seismological data: Bulletin of Volcanology, v. 67, p. 358–369, doi:10.1007/s00445-004-0381-7.

Caprarelli, G., Tsutsumi, M., Turi, B., 1997, Chemical and isotopic signature of the basement rocks from the Campi Flegrei geothermal field (Naples, southern Italy): inferences about the origin and evolution of its hydrothermal fluids: Journal of Volcanology and Geothermal Research, v. 76, p. 63–82.

Carlino, S., Piochi, M., Troise, C., Tramelli, A., Scheu, B., Mayer, K., Montanaro, C., Mormone, A., Somma, R., De Natale, G., in preparation, Small scale and large scale permeability of rocks in volcanic areas: new insight on Campi Flegrei caldera (Southern Italy) from bore-hole data and laboratory experiments.

Chiodini, G., Baldini, A., Barberi, F. , Carapezza, M. L., Cardellini, C., Frondini, F., Granieri, D. , and Ranaldi, M., 2007, Carbon dioxide degassing at Latera caldera (Italy): Evidence of geothermal reservoir and evaluation of its potential energy: Journal Geophysical Research, v. 112, B12204, doi:10.1029/2006JB004896.

Chiodini, G., Frondini, F., 2001, Carbon dioxide degassing from the Albani Hills volcanic region, Central Italy: Chemical Geology, v. 177, p. 67–83.

Chiodini, G., Frondini, F., Cardellini, C., Granieri, D., Marini, L., Ventura, G., 2001, CO_2 degassing and energy release at Solfatara volcano, Campi Flegrei, Italy: Journal of Geophysical Research B, Solid Earth, v. 106 (B8), p. 16213-16221.Mazot, A., Rouwet, D., Taran, Y., Inguaggiato, S., Varley, N., 2011, CO_2 and He degassing at El Chichón volcano, Chiapas, Mexico: gas flux, origin and relationship with local and regional tectonics: In Inguaggiato, S., Shinohara, H., and Fischer, T. (eds) Geochemistry of volcanic fluids: a special issue in honor of Yuri A. Taran: Bulletin Volcanology, v. 73(4), p. 423–442.

Mazot, A., Schwander, F., Christenson, B., de Ronde, C. E.J., Inguaggiato, S., Scott, B., Graham, D., Britten, K., 2014, CO_2 discharge from the bottom of volcanic Lake Rotomahana, New Zealand: G3 v. 15, 3. doi: 10.1002/2013GC004945.

Mormone, A., Troise, C., Piochi, M., Balassone, G., Joachimski, M., De Natale, G., 2015, Mineralogical, geochemical and isotopic features of tuffs fromthe CFDDP drill hole: Hydrothermal activity in the eastern side of the Campi Flegrei volcano (southern Italy): Journal Volcanology Geothermal Research http://dx.doi.org/10.1016/j.jvolgeores.2014.12.003.

Pérez, N.M., Hernández, P.A., Padilla, G., Nolasco, D., Barrancos, J,. Melián,, G., Padrón, E., Dionis, S., Calvo, D., Rodríguez, F., Notsu, K., Mori, T.,Kusakabe, M., Arpa, M.C., Reniva, P., Ibarra ,M ., 2011, Global CO_2 emission from volcanic lakes: Geology, v. 39(3), p. 235–238, doi:10.1130/G31586.1.

Perez, N.M., Hernandez, P.A., Padron, E., Melin, G., Nolasco, D., Barrancos, J., Padilla, G., Calvo, D., Rodriguez, F., Dionis, S., Chiodini, G. , 2013, An increasing trend of diffuse CO_2 emission from Teide volcano (Tenerife, Canary Islands): Geochemical evidence of magma degassing episodes: Journal of the Geological Society, v. 170 (4), p. 585-592.

Rosi, M., & Sbrana, A., 1987, Phlegrean Fields. CNR, Quaderni Ricerca Scientifica 114, 175 pp.

Sinclair, A.J., 1974, Selection of threshold values in geochemical data using probability graphs: Journal of Geochemical Exploration, v.3, p. 129 -149.

Sorey, M.L., Evans, W.C., Kennedy, B.M., Farrar, C.D., Hainsworth, L.J., Hausback, B., 1998, Carbon dioxide and helium emissions from a reservoir of magmatic gas beneath Mammoth Mountain, California: Journal Geophysical Research, v. 103, p. 15303-15323.

Viveiros, F., Cardellini, C., Ferreira, T., Caliro, S., Chiodini, G. , and Silva C., 2010, Soil CO_2 emissions at Furnas volcano, São Miguel Island, Azores archipelago: Volcano monitoring perspectives, geomorphologic studies, and land use planning application: Journal Geophysical Research, v. 115, B12208, doi:10.1029/2010JB007555.

Werner, C., and Brantley, S., 2003, CO_2 emissions from the Yellowstone volcanic system, Geochemistry Geophysics Geosystems, v. 4, 1061, doi:10.1029/2002GC000473.

Werner, C., Cardellini, C., 2006, Comparison of carbon dioxide emissions with fluid upflow, chemistry, and geologic structures at the Rotorua geothermal system, New Zealand: Geothermics, v. 35 (3), p. 221-238.